Energy Conversion and Management 157 (2018) 498–510

Contents lists available at ScienceDirect

Energy Conversion and Management

journal homepage: www.elsevier.com/locate/enconman

CFD modelling development and experimental validation of a phase change material (PCM) heat exchanger with spiral-wired tubes

W. Youssef, Y.T. Ge*, S.A. Tassou

RCUK National Centre for Sustainable Energy Use in Food Chains (CSEF), Institute of Energy Future, Brunel University London, Uxbridge, Middlesex UB8 3PH, UK

ARTICLE INFO

Keywords:
Solar assisted heat pump
PCM heat exchanger
CFD modelling
Model validation and application

ABSTRACT

Employing phase change materials (PCMs) for latent heat storage (LHS) application has a great potential to improve a solar thermal system performance. Despite this fact, the use of PCM in this area is quite limited due to the poor thermal conductivity of available PCMs. Therefore, heat transfer enhancement is one of the essential strategies that can overcome this obstacle. In this paper and related project, a PCM heat exchanger (HX) is purposely designed with spiral-wired tubes and integrated in an indirect solar assisted heat pump test system. Although the spiral-wired tube has not been applied in a PCM HX, it is expected to enhance significantly the PCM heat transfer and heat storage performance. To verify this and understand the PCM heat storage and releasement processes, a detailed 3D CFD model has been developed for the PCM HX and validated with measurements. The temperature variations and visualizations of the PCM during charging and discharging processes are therefore simulated and presented temporally. Furthermore, the effects of different inlet heat transfer fluid flow rates and temperatures on the PCM melting/solidification time are demonstrated in this study. Some significant simulation results have been obtained which can instruct efficiently the operation of the heat exchanger and its integration with the solar system.

1. Introduction

Solar thermal systems have been widely applied in domestic hot water production due to their sustainability and stability in operations. In these kinds of systems, thermal energy storage technologies and utilizations are essential considering the intermittent nature of solar energy resource. The energy storage technologies can be classified as sensible heat, thermochemical and latent heat storages [1]. For the sensible heat storage, the amount of heat stored is dependent on the production of the material's mass, specific heat and temperature change such that a larger vessel and bigger installation space are normally required. For the thermochemical storage, it consists of a series of reversible reactions to store and release heat energy [2]. This technology offers higher energy density than those of sensible or latent heat storage systems. However, it is still at the stage of research and development. As to the latent heat storage, it involves phase change material (PCM) changed from one state to another such as solid to liquid, liquid to solid or solid to solid when heat is added or released. The applicable PCMs include organic, inorganic and eutectic materials with different melting and solidification temperature points [3,4]. The organic PCMs, such as fatty acids and paraffin, have self-nucleating properties but lower thermal conductivity and higher cost [5]. Such PCMs have been successfully applied to many domestic and commercial installations such as space heating in buildings, solar air/water heating and refrigeration systems, etc. [6]. The inorganic materials such as salt hydrates have good availability and lower cost but exhibit difficulties in phase separation and hard to be melt incongruently. The eutectic PCMs are composed of either organic materials or inorganic materials or their mixtures [6]. Nevertheless, a eutectic PCM tends to be a solution of salt in water that has a phase change temperature below 0 °C. It is therefore important to select the optimal PCM in any particular application to satisfy practical requirements of operation and cost. Comparing to those sensible heat storages, the solid-liquid latent heat storage systems can be more compact due to the high latent heat values of PCMs. However, the most undesirable property of a PCM is its low thermal conductivity which can affect its wide applications in a latent heat storage system. The heat transfer enhancement in a PCM is thus essential.

Different heat transfer enhancement methods for PCMs were proposed by researchers [7–10]. Some of these methods suggested the use of fins while the others recommended mixing randomly the PCM with high thermal conductivity particles such as carbon fibres and metal beads. Of these possible heat transfer enhancement methods, enhancements with fins were found to be the feasible solutions due to their simpler designs, easier manufacturings, lower cost and higher

* Corresponding author.
E-mail address: Yunting.Ge@brunel.ac.uk (Y.T. Ge).

https://doi.org/10.1016/j.enconman.2017.12.036
Received 3 October 2017; Received in revised form 9 December 2017; Accepted 11 December 2017
Available online 18 December 2017

Nomenclature

A	area (m^2)
C	constant
Cp	specific heat capacity (kJ/kg·K)
f	friction factor
$\overline{h}$	convection heat transfer coefficient of HTF (W/m^2·K)
h	sensible enthalpy of PCM (kJ/kg)
H	total enthalpy of PCM (kJ/kg)
K	thermal conductivity (W/m·K)
L	latent heat of PCM (kJ/kg)
l	total pipe length (m)
$\dot{m}$	mass flow rate (kg/s)
Nu_D	Nusselt number
Pr	Prandtl number
Q	heat capacity (kW)
r	radius (m)
Re_D	Reynolds number
s	shape factor
S	momentum source term (pa/m)
T	temperature (°C)
t	time (s)
$\vec{u}$	component velocity (m/s)
w	width (m)

Greek symbols

ρ	fluid density (kg/m^3)
β	liquid fraction
μ	dynamic viscosity (kg/m·s)

Subscripts

c	copper
i	inside
in	HTF Inlet
liqu	at liquid state
lm	log-mean difference
mush	Mushy zone
o	outside
out	HTF Outlet
pcm	phase change material
ref	reference
s	surface
solid	at solid state
w	water
wf	water fluid

efficiency [9]. Further, the PCM heat transfer enhancements were compared experimentally when circular and longitudinal fins were applied [11]. Subsequently, the PCM with longitudinal fins presented better performance since the enhancement with longitudinal fins showed 12.5% decrease in melting time for 80 °C inlet heat transfer fluid (HTF) temperature. On the other hand, the use of triplex tube heat exchanger with different fin configurations demonstrated that the parameters of fin length, number and pitch had strong effects on the melting time of PCM [12,13]. Nonetheless, the heat transfer enhancement performance for a particular application also depends on some other parameters such as application configuration, heat transfer fluid and type of PCM etc. In one of the relevant studies, different types of PCM heat exchanger (HX) designs were selected [14]. These included double pipe HX with PCM in the annular space or embedded in a graphite matrix, double pipe HX with external fins on the copper tube and PCM in the annular space, compact HX with PCM between coil and fins, and plate and frame HX with PCM in half of the passages. The experimental investigations showed that the double pipe HX with PCM embedded in graphite matrix presented the highest overall heat transfer coefficient while the compact HX could provide the highest average thermal power due to its highest ratio of heat transfer area to external volume. Consequently, there are many design and operating options which can affect the PCM heat transfer enhancements. It is therefore necessary to find out an efficient method to evaluate, compare and optimise these options.

Dynamic models based on enthalpy method were developed for a solar assisted PCM cylindrical energy storage tank [15,16]. The models were further compared and validated with corresponding experimental results [17]. The research outcomes showed that some important design and operating parameters could affect significantly the performance of the PCM energy storage tank. These included storage tank structures, PCM types and temperature and flow rate of heat transfer fluid (HTF), etc. Of those applicable design and evaluation methods, CFD modelling can be an efficient simulation tool to predict the melting/solidification behaviour of PCM by numerically solving Navier-Stokes partial differential equations of mass, energy and momentum [18]. This can be achieved using the enthalpy method which determines the enthalpy value in the energy equation. The total enthalpy value covers both sensible and latent parts in which the latent enthalpy is evaluated as a percentage of the latent heat of the PCM in liquid phase state. Alternatively, this percentage is also known as liquid fraction of the PCM [18]. Comparing to the experimental investigations, the CFD modelling strategies have a number of advantages in terms of less time consuming and more designed options to be evaluated. With a validated CFD model, some significant and detailed simulation results can be obtained. These include dynamic profiles of PCM temperature, melting/solidification rate, heat transfer rate and energy stored/released, etc. However, to set up an accurate CFD model for the PCM heat exchangers, some important parameters need to be specified such as the equivalent thermal conductivity when some heat transfer enhancement materials are mixed with the PCM. In addition, an appropriate phase change model to characterise the PCM melting and solidification behaviours need to be selected in the CFD model of which the model of "volume of fluid" was commonly applied [19,20]. Even so, some other phase change models may be evaluated and compared.

It is understood from literature reviews that some technologies can enhance the heat transfer of PCM for heat storage such as PCM with longitudinal fins or PCM embedded with graphite matrix. However, these designs can also block somewhat the movement of PCM during phase change processes which conversely affect the further heat transfer enhancement of PCM. Subsequently, in this project, a PCM heat exchanger was purposely designed in which a number of spiral-wired tubes were equipped to enhance the PCM heat transfer. To the authors' knowledge, the spiral-wired tube has not been applied so far in the heat transfer enhancement of PCM and the application of energy storage is a solar thermal system. The special structures of spiral-wired tubes can not only improve the thermal conductivity of PCM but also allow free movement of PCM during phase change processes which can further enhance the PCM heat transfer. To evaluate and analyse the PCM heat transfer behaviours of the proposed PCM heat exchanger in an application of an indirect solar assistant heat pump (IDX-SAHP), a detailed 3D CFD model has been developed for the heat exchanger (HX). Special treatments are considered in the CFD modelling such as the equivalent thermal conductivity calculations, etc. The developed CFD model has been validated with experimental measurements and simulations are therefore carried out at different operating conditions. The simulation results are significant to understand the working mechanism of PCM melting/solidification process and effect of operating conditions on the

PCM HX performance and thus optimising the heat exchanger operation.

2. Experimental setup

The PCM HX was designed to be employed in an indirect expansion solar assisted heat pump (IDX-SAHP) system for hot water production [21]. Therefore, the PCM melting/solidification temperature, the HX capacity, Heat transfer fluid (HTF) inlet flow rate and inlet temperatures were selected based on this application. More detailed introductions about the experimental setup for the IDX-SAHP test rig can be found out from our previous publication [21]. The published experimental work, however, did not describe in detail the design, operation conditions of the PCM HX and the PCM selection. Therefore, in this paper, a detailed description of the PCM HX design and manufacturing process is presented. The temperature sensors are all 10 K thermistor type with the range and accuracy of −55 °C to 125 °C and ± 0.1 °C respectively. The flow rate sensor is pulsed-screwed water meter with the range and accuracy of 35 L/h to 7000 L/h and ± 5% each.

2.1. PCM material selection

Based on previous literatures, organic PCMs have shown more stability and efficiency in energy charging and discharging lifecycles. It is therefore quite suitable for the application of a SAHP heating system. Correspondingly, the selected phase change material in this study was organic paraffin type A16 which has a melting point temperature 16 °C. This temperature was selected based on the following considerations: (i) The PCM HX takes a role of heat source to the evaporator of the solar heat pump. (ii) The UK weather is not always sunny and solar irradiance is not high, therefore, the PCM can be charged as much as possible from the solar collector, especially during winter time period. (iii) During summer, the ambient temperatures in the UK climate can be above 18 °C. This allows ambient heat to be charged. After searching from the current product market, the properties of the selected PCM and the melting/solidification cycle are described in Table 1.

2.2. Design of PCM HX charge

After selecting the PCM material, it was quite challengeable to find out the matched weight charge of PCM for the experimental rig based on the required energy to be stored. The aim of the PCM HX was to store excessive solar or ambient energy and be used as a heat source for the IDX-SAHP system. The designed evaporator cooling capacity of the heat pump unit was 2 kW so as to produce sufficient heating to the water storage tank through the heat pump condenser. With this capacity, the PCM energy (dominantly latent energy) was expected to be stored or released within a specified time period and calculated as Eq. (1):

$$E = m \times L = Q \times \Delta t \quad (1)$$

The time period was set to 1 h such that the required PCM weight charge was 33.8 kg. Subsequently, 35 kg PCM was ordered and charged in the PCM HX.

2.3. Heat transfer enhancement and detailed design

The HTF used in the experiment and CFD modelling was a mixture of glycol water with glycol concentration of 25% (Wt). The enhancement design was based on a spiral-wired tube which had copper wires soldered around the main copper tube as shown in Fig. 1.

After calculating the amount of PCM mass, the PCM volume was determined by the density of the PCM. A few designs were initially considered and drawn in SolidWorks including solenoidal, cylindrical and spherical tanks. For the optimal use of the tank volume, a full detailed tank structure has been evaluated using SolidWorks as shown in Fig. 2. As the manufacturing process was conducted via the lab facilities at Brunel University, a rectangular mild steel container was found reasonable and easy to make as the exterior for the PCM HX. The reason to choose mild steel is because it is cheap and has low thermal conductivity. A mild steel sheet was folded and welded according to the detailed drawing from SolidWorks. The container was designed to contain eight of the proposed spiral-wired tubes. As shown in Fig. 2 (left), the container has eight 22 mm diameter holes at both top and bottom in order to fit the spiral-wired tubes through it. The container top cover was designed to be removable so as to fill or discharge the PCM material. The spiral-wired tubes at both top and bottom ends were connected by a number of U-shape silicon connectors, as shown in Fig. 2. As the U-shape silicon connectors contribute with small internal area compared with the overall internal area of the spiral tubes, the heat transfer effect between the HTF and ambient was neglected in the numerical model, especially they are not in contact with the PCM. These silicon connectors were selected because they are flexible and can withstand high pressure and temperature.

After a fully detailed drawing was completed based on the proposed design, the manufacturing process took place. As shown in Fig. 3, after folding and welding the mild steel sheet, eight holes were drilled at the bottom of the container. The spiral-wired tubes were laid off in the container and the bottom ends of the spiral-wired tubes were soldered to the container body. A thermistor was placed inside the tank close to the middle to measure the internal temperature of the PCM. Then a black rubber sealant was placed between the top cover and container body. After that, the U-shape silicone connections were fitted at both bottom and top of the container. Another thermistor was placed at the exterior front of the container to measure the temperature change at different places of the HX. Finally, it was really important to insulate that exterior of the PCM HX to minimize the heat losses such that a 50 mm thick insulation was attached to the HX exterior. The PCM was filled into the PCM HX during the previous process.

3. Mathematical and numerical methodology

3.1. Heat transfer fluid (HTF)

In order to simulate the copper spiral-wired tube and its effect on the heat transfer enhancement between the HTF and PCM, an estimation method is proposed to evaluate the overall thermal conductivity for the PCM when the effect of the spiral wires is considered. This method is proposed because of the compact design of the spiral-wired tube which makes the CFD meshing elements enormous and simulation time extremely long. As shown in Fig. 4, the fin wires are really small in size compared with the main body of the pipe. Therefore, it is considered to evaluate the PCM thermal conductivity including the effect of the finned wires as one element. It is also assumed that the PCM HX could be divided into eight rectangle tube sections. At each section, the HTF pipe is centred in the middle of this section, as shown in the red rectangle in Fig. 4. Also, the flowing assumptions are considered for this calculation:

Table 1
PCM-A16 properties.

Properties	Values	Units
Melting temperature range	15–17	°C
Congealing temperature range	17–15	°C
Latent heat	213	$kJ{\cdot}kg^{-1}$
Specific heat capacity	2.3–2.37	$kJ{\cdot}(kg{\cdot}K)^{-1}$
Density of solid (at 10 °C)	830	$kg{\cdot}m^{-3}$
Density of liquid (at 25 °C)	800	$kg{\cdot}m^{-3}$
Thermal conductivity	0.18	$W{\cdot}(m{\cdot}K)^{-1}$
Flash point	> 250	°C
Max operation temp.	200	°C

Fig. 1. Copper spiral-wired tube.

- Steady-state conditions.
- Incompressible liquid and negligible viscous dissipation.
- Constant properties.
- Neglect natural convention effect for the PCM.
- The spiral wires are distributed equally across the PCM.

Fig. 5 shows a section from the spiral-wired tube and its analysis. During the PCM discharging condition in which the HTF inlet temperature is lower than the PCM temperature inside the PCM HX, the heat will be transferred from the PCM to the pipe wall through conduction and then to the HTF through convection. By knowing the HTF flow rate and inlet and outlet HTF temperatures of the PCM HX from the experimental results, the total amount of thermal power transferred to the tank can be evaluated; this thermal power is transferred constantly between the HTF and the PCM. Therefore, as listed in Eq. (2), the overall PCM thermal conductivity (k_{pcm}) can be evaluated. During convection heat transfer, the convection heat transfer coefficient was calculated by knowing the Nusselt number, the internal diameter of the pipe and the thermal conductivity of the fluid as listed in Eq. (3). The Nusselt number depends on the Reynolds number, Prandtl number and internal friction factor (f) of the surface as listed in Eq. (4) in which the friction factor (f) is calculated as Eq. (5). The log-mean temperature difference is calculated using Eq. (6). The inside surface temperature of the copper pipe can therefore be determined by solving the Eqs. (2)-(6).

The third term of the Eq. (2) determines the outside surface temperature of the copper pipe. The last term of the Eq. (2) determines the overall conduction coefficient of the PCM. This can be evaluated by knowing the shape factor (s) which can be calculated using Eq. (7) [22]. The effective PCM thermal conductivity coefficient including the wires effect is calculated at 11.07 W/(m·K) when the HX structural data and boundary parameters are given.

$$Q = \underbrace{[\dot{m}_{wf} Cp_{wf}(T_{in}-T_{out})]}_{main\ heat\ transfer} = \underbrace{[\bar{h}A_s\Delta T_{lm}]}_{Convection} = \underbrace{\left[\frac{2\pi k_c l}{\ln\left(\frac{r_{c,o}}{r_{c,i}}\right)}(T_{s,i}-T_{s,o})\right]}_{Pipe\ Conduction} = \underbrace{[sk_{pcm}(T_{s,o}-T_{pcm})]}_{PCM\ conduction} \quad (2)$$

where the convection heat transfer coefficient expressed by:

$$\bar{h} = Nu_D \frac{k_w}{2r_{c,i}} \quad (3)$$

$$Nu_D = \frac{\left(\frac{f}{8}\right)(Re_D-1000)Pr}{1+12.7\left(\frac{f}{8}\right)^{\frac{1}{2}}\left(Pr^{\frac{2}{3}}-1\right)} \qquad 0.5 \leqslant Pr \leqslant 2000; 3000 \leqslant Re \leqslant 5\times 10^6 \quad (4)$$

$$f = (0.790\ln Re_D - 1.64)^{-2} \qquad 3000 \leqslant Re \leqslant 5\times 10^6 \quad (5)$$

and the log-mean temperature difference expressed by:

$$\Delta T_{lm} = \frac{(T_{s,i}-T_{out})-(T_{s,i}-T_{in})}{\ln\left(\frac{(T_{s,i}-T_{out})}{(T_{s,i}-T_{in})}\right)} \quad (6)$$

$$s = \frac{2\pi l}{\ln\left(1.08\frac{w}{2r_{c,o}}\right)} \quad (7)$$

3.2. PCM

A 3D CFD dynamic model for the PCM HX is developed using ANSYS® Fluent. As shown in Fig. 6, the model is set up firstly on Solidworks® before being imported into ANSYS® to be modelled, meshed and posted. The CFD model is developed to study the effects of different HTF flow rates and temperatures on the melting and solidification processes of the PCM with the proposed heat transfer enhancement method. For melting process solver equation, the following assumptions

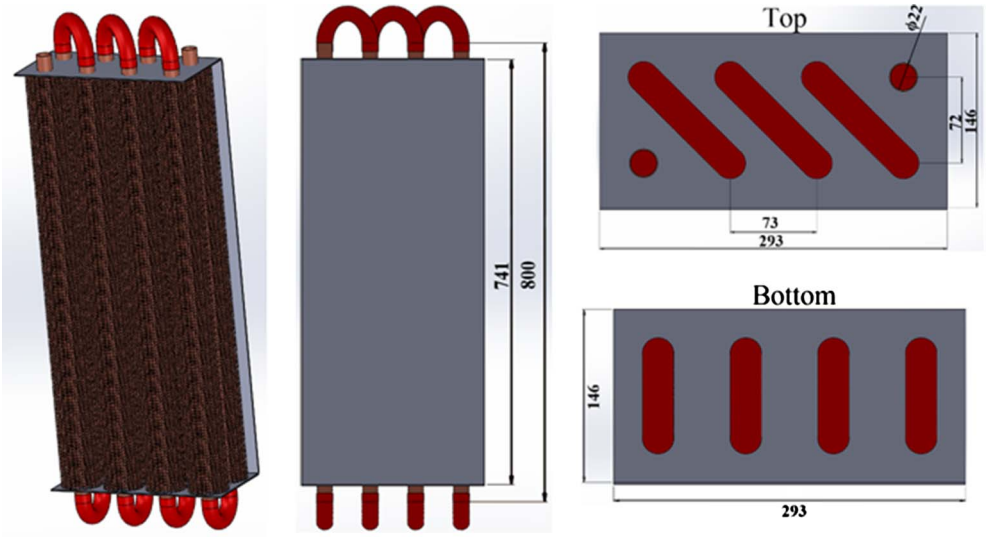

Fig. 2. 3D drawing in mm for PCM HX – Isometric (left) – front (middle) – top and bottom (right).

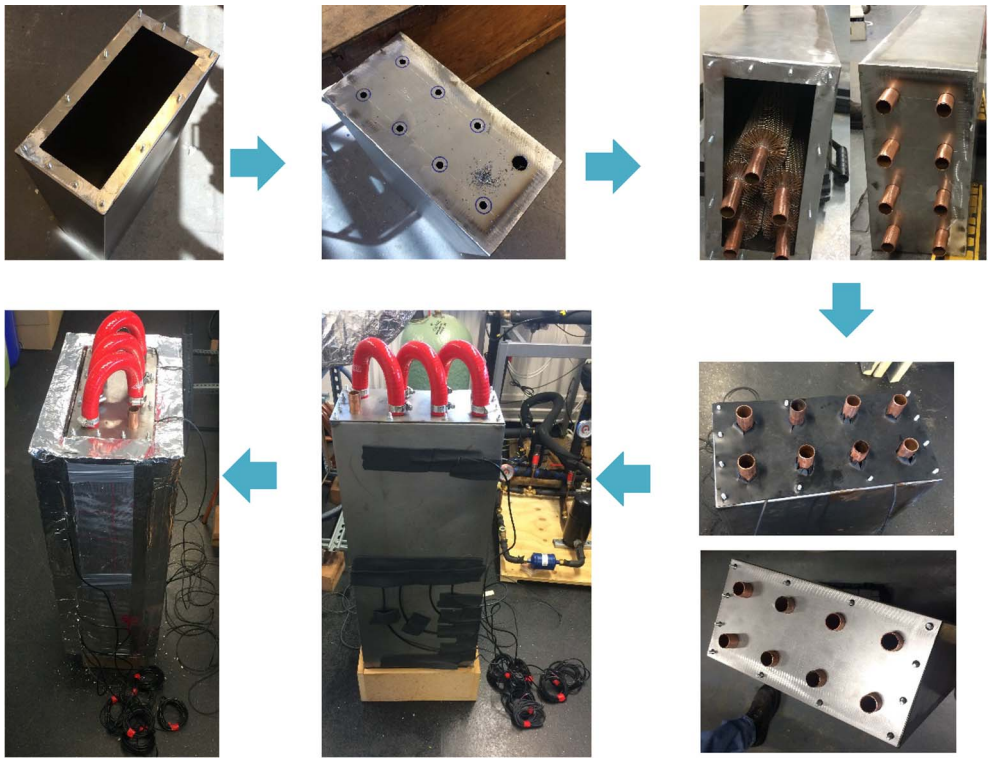

Fig. 3. PCM HX design process.

are considered:

- The flow is laminar, unsteady, and incompressible.
- The viscous dissipation is considered negligible.
- The effect of natural convection during melting is considered by invoked the Boussinesq approximation which is valid for the density variations buoyancy force, otherwise, they are neglected.
- The thermo-physical properties of the HTF and PCMs are independent of the temperature.

Continuity equation:

$$\frac{\partial}{\partial t}(\rho) + \nabla\cdot(\rho\vec{u}) = 0 \tag{8}$$

Momentum equation:

$$\frac{\partial}{\partial t}(\rho\vec{u}) + \nabla\cdot(\rho\vec{u}\,\vec{u}) = \mu\nabla\cdot\vec{u} - \nabla P + \rho\vec{g} + S \tag{9}$$

where S is the momentum source term due to the reduced porosity in the mushy zone and can be expressed as:

$$S = \frac{(1-\beta)^2}{(\beta^3 + \epsilon)} C_{mush}\,\vec{u} \tag{10}$$

where ϵ is a small number (0.001) to prevent division by zero, C_{mush} is the mushy zone morphology constant. This constant measures the amplitude of the damping and describes how steeply the velocity is reduced to zero when the material solidifies. This constant should be in the range of 10^4–10^7 [23] such that10^5 are chosen in this study.

Energy equation:

$$\frac{\partial}{\partial t}(\rho H) + \nabla\cdot(\rho\vec{u}H) = \nabla\cdot(K\nabla T) \tag{11}$$

The melting-solidification processing is evaluated by defining the liquid fraction (β) quantity. This considers the fraction of liquid at each cell in the PCM domain. The liquid fraction is determined based upon

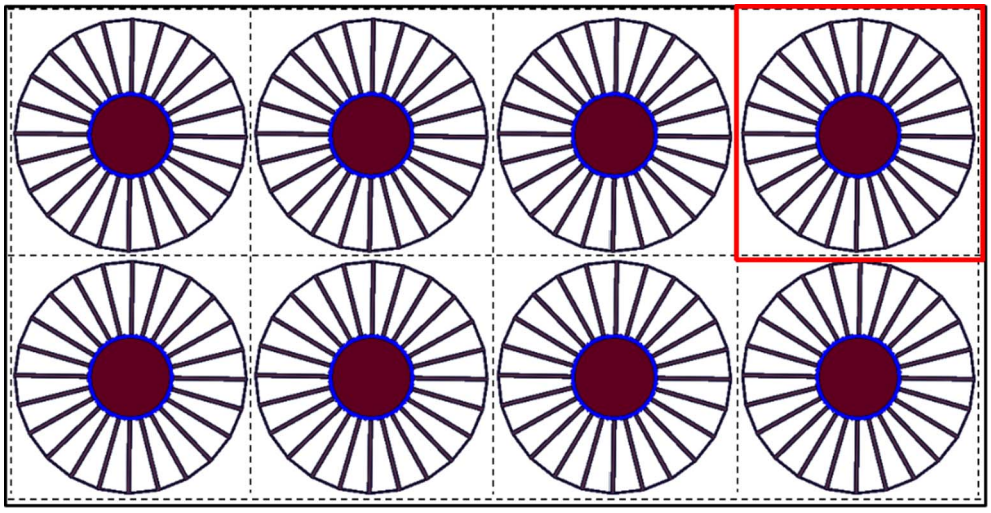

Fig. 4. PCM HX sections.

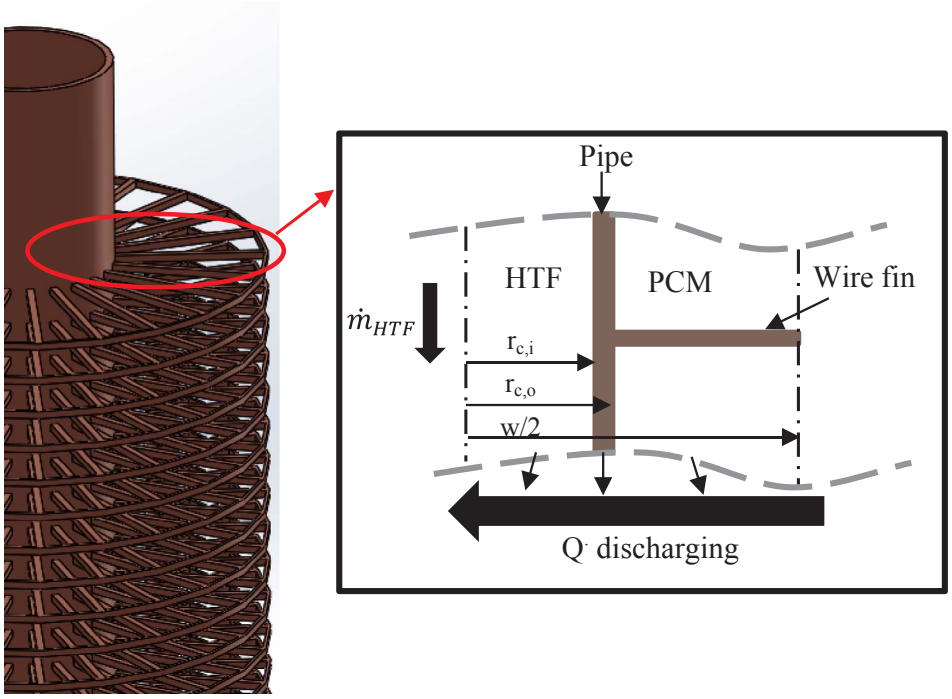

Fig. 5. Spiral-wired tube element analysis.

the enthalpy (H) balance at each cell. As explained in Eq. (12)-(15).

$$h = h_{ref} + \int_{T_{pcm,ref}}^{T_{pcm}} Cp_{pcm}\,dT \tag{12}$$

where h is the sensible enthalpy, h_{ref} is the reference enthalpy at the reference temperature T_{ref} and Cp is the specific heat.

$$H = h + \Delta H \tag{13}$$

where ΔH is the latent heat that may change between the solidification and melting processes.

$$\beta = \Delta H / L \tag{14}$$

where β the liquid fraction. The liquid fraction can be expressed in terms of temperatures as:

$$\beta = \begin{cases} 0 & if\ T_{pcm} < T_{pcm,solid} \\ 1 & if\ T_{pcm} > T_{pcm,liqu} \\ \frac{T_{pcm} - T_{pcm,solid}}{T_{pcm,liqu} - T_{pcm,solid}} & if\ T_{pcm,liqu} > T_{pcm} > T_{pcm,solid} \end{cases} \tag{15}$$

where T_{solid} is the temperature of the PCM when the last liquid content is solidified and T_{Liqu} is the temperature of the PCM when the last solid content is liquefied.

The PCM material properties are defined in Table 1 but its thermal conductivity is revised and calculated by the formulas explained in Section 3.2 considering the heat transfer enhancement of fin wires. The

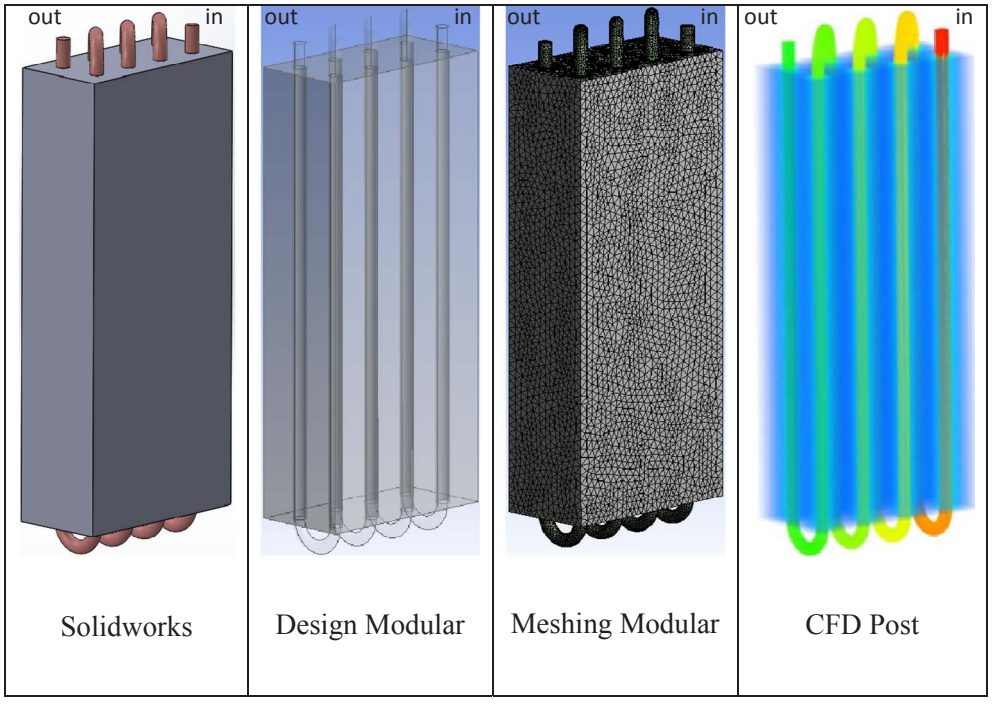

Fig. 6. PCM HX numerical model development.

HTF properties are imported from the CFD Fluent built-in database and the standard k-ε turbulence model with standard wall functions is applied. The multiphase function is enabled and "Volume of Fluid" model is selected with implicit volume of fraction parameters and pull velocity enabled. The PISO scheme is used for pressure-velocity coupling. The spatial discretization settings for pressure, momentum, volume of fraction and energy are PRESTO, first order unwind, compressive and second order unwind respectively. The under relaxation value factors for pressure, density, momentum, energy, and liquid fraction are 0.3, 1, 0.7, 1 and 0.9 respectively. The predetermined convergences of energy and velocity are 10^{-4} and 10^{-3} respectively.

For the initial conditions of charging process, the PCM and HTF temperatures are set to 10 °C and 40 °C respectively and PCM is in solid state. On the other hand, for the initial conditions of discharging process, the PCM and HTF temperatures are set to 40 °C and 10 °C each and PCM is in liquid state. As to the boundary conditions of the CFD model, the type of "Velocity-inlet" is used for the HTF at the PCM HX inlet. The inlet HTF flow velocity is determined from the inlet volumetric flow rate and inlet inner pipe diameter. The HTF flow rates vary from 0.1 L/s to 0.3 L/s for both charging and discharging processes while the HTF flow temperatures change from 30 °C to 50 °C for charging process and 5–15 °C for discharging process. The HTF outlet boundary condition is selected as "outflow". In addition, since the PCM HX outer surface was well insulated, its boundary condition is set as adiabatic.

Being a 3D simulation, it is important to develop a simulation method to minimize the simulation time. As the HTF flow rate is constant for each simulation, the model is first initialized as steady-state to evaluate the flow and turbulence effect. After the solutions are converged, the transient simulation is activated by enabling the energy and volume fraction equations only.

Table 2
Mesh selection – coarse and fine.

Level	No of elements	No of nodes	Skewness	Time per iteration
Coarse	920703	244452	Av: 0.23%, stdev: 0.12%	6–11 s
Fine	1981116	514875	Av: 0.22%, stdev: 0.12%	9–13 s

3.3. Meshing dependency and model validation

To ensure the simulation quality, the mesh selection is necessary to obtain the best results. This is investigated by comparing two different mesh levels: coarse and fine as shown in both Fig. 7 and Table 2. The cell types used in both meshes are tetrahedron across the whole model but wedge at the inflation layers. The main purpose of the inflation layers is to enhance heat transfer simulation between the HTF and PCM. The fair skewness range of the mesh must not exceed 0.5–0.75 [19].

The simulations for both meshes are conducted to compare the outcome results. The results are quite close to each other where maximum and average relative errors are 1.6% and 0.08% respectively. Taking the simulation time into consideration, the simulation with coarse mesh is found faster than that with fine mesh to reach convergence during initialization as steady state and also during transient

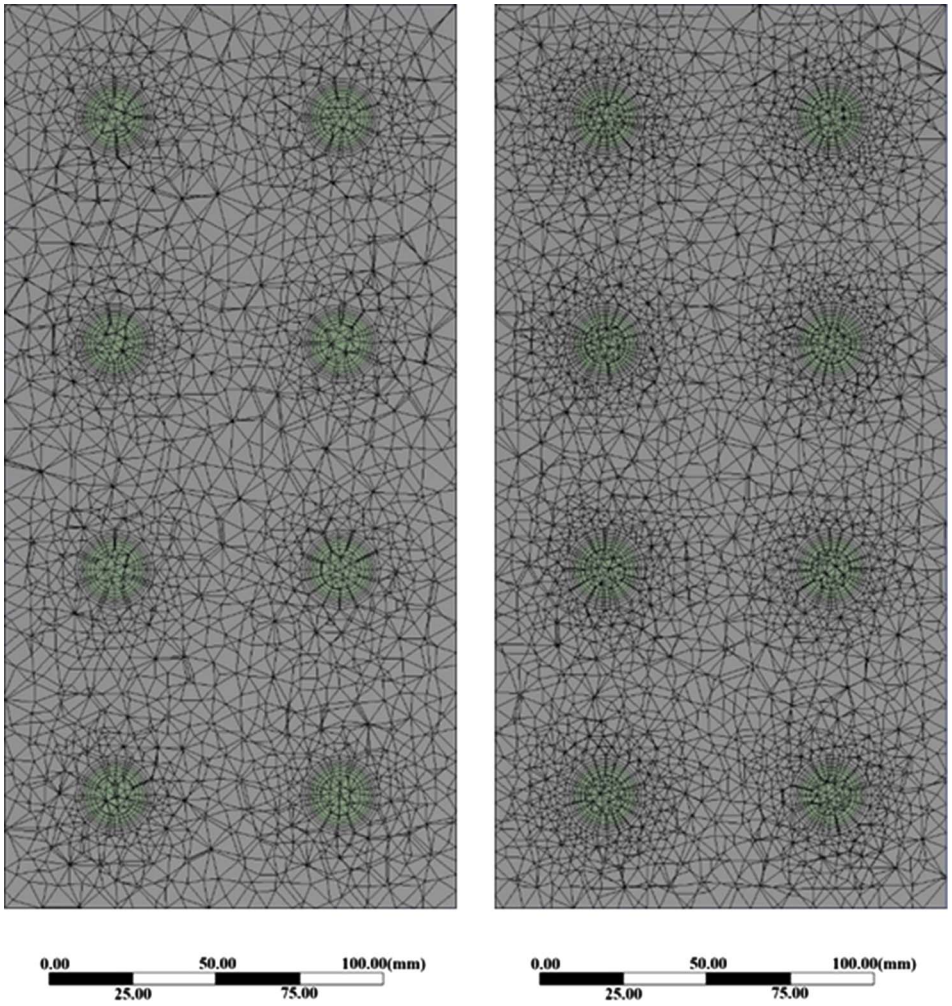

Fig. 7. Mesh comparison of PCM HX horizontal cross-section – coarse and fine, respectively.

simulation. Therefore, the CFD model with coarse mesh is more suitable to be validated with the experimental results as it has fewer elements number. During Transit modelling, time intervals of 1 s, 5 s, and 10 s are tried and compared to find out an appropriate time interval. The simulation results show less than 5% difference when time intervals of 1 s and 5 s are applied. Subsequently, 5 s time interval is selected for the model to save computing time.

Fig. 8 shows the comparisons between the experimental and CFD simulation temperatures of a generic thermistor in the middle of the tank during discharging and charging processes. The HTF mass flow for the simulation and experiment during both charging and discharging processes is set at 0.1 L/s. Meanwhile, the inlet HTF temperatures during charging and discharging processes are set at 40 °C and 10 °C respectively. During discharging, it is observed that the PCM was sub-cooled at the beginning of the phase change process during the test but it does not appear in the simulation result. That is because the solver does not take sub-cooling effect into account. The absolute errors are calculated during the discharging process with the maximum and average values of 3.59 K and 0.75 K respectively. Meanwhile, the absolute errors during charging process are also evaluated with the maximum and average values of 1.38 K and 0.51 K respectively. Since the absolute errors are all less than 3.59 K, the validation of the CFD model can be considered to be acceptable [24].

4. Model applications

4.1. PCM temperature contours at charging and discharging processes

The developed 3D CFD model of the PCM HX is used to predict and analyse the effects of varied HTF inlet flow rate and temperature on the heat exchanger charging and discharging processes and behaviours.

Fig. 9 shows the PCM liquid mass fraction, temperature and total energy at the mid of charging and discharging processes. It is observed that at the specified operating conditions the charging process is much quicker than that of discharging one. During the charging process, initially, the heat transfers from the HTF to the PCM through pure conduction. When the PCM starts to melt, the natural convection heat transfer between the liquefied PCM and pipe outer surface will directly affect the charging time. Also, the buoyancy effect adds a little convection due to PCM density variation. Again in this Figure, for the charging process, the PCM liquid mass fraction decreases radically from each pipe outer surface while at each cross section more liquid contents are existed close to the inlet pipe due to relatively higher HTF temperature. Correspondingly, similar distribution profile can be found for the total energy. However, the PCM temperatures across the tank are much evenly distributed at a range of 16–17 °C due to the co-existed of liquid and solid phases at that time. Similar parameter distributions can also be established for the discharging process except that the larger liquid mass fraction and total energy are higher at the places close to the outlet pipe due to the higher HTF temperatures. Again, during the discharging process, it is noted that the PCM HX takes longer time to release the stored energy. This can be further explained by the following evidences. When the stored heat transfers from PCM HX to the HTF, the first solidification layer starts to accumulate on the outer surface of the copper tube and the spiral wires. This will create an extra conduction thermal resistance in the heat transfer path between the two domains. With the increase of solid content, such thermal resistance will increase as well. On the other hand, neither natural convection nor buoyancy effect exists during the discharging process as the solid content is uniformly accumulated along the spiral-wired tubes. Furthermore, it is noted that the absolute temperature differences between PCM phase change and HTF temperature are roughly 25 K for charging process and 5 K for discharging process respectively. The larger temperature difference can also contribute the quicker PCM phase change process in charging.

Fig. 10 shows the CFD temporal variation of the PCM temperature at top, middle and bottom of the PCM HX during charging process at various times from start: 30 s, 270 s, 1050 s, 1950 s and 2520 s. The inlet HTF (right-bottom of the first figure in each row) temperature and flow rate are maintained at 40 °C and 0.1 L/s respectively. At the start of the process (at 30 s), the temperature distribution across the PCM HX is fairly uniform. At 270 s, it is observed a sudden rise in the PCM temperature from 10 °C to 16 °C. That is due to the high-temperature difference at the beginning between the PCM and HTF and simultaneously sensible heat transfer when the PCM temperature is below its melting point. After that when the PCM reaches its melting temperature, the PCM starts to melt around the spiral-wired tubes and grows radially towards the middle of the tank and the edges. At the mid of the charging time (1050 s), more areas around each tube are liquefied and temperatures are well above the melting point although the PCM temperature decreases gradually away from each tube outer surface. Even so, approximately 50% of tank volume is still occupied with solid PCM based on the temperature distributions. At time 1950 s, over 90% of the PCM in the tank is liquefied and the liquid PCM temperature follows the HTF temperature distribution inside the pipe. At the end of the charging process (at 2520 s), PCM in the tank is completely liquefied. Meanwhile, the PCM temperatures inside the tank reach their highest values and their distributions all follow the temperature profile of HTF inside the pipes.

Similarly, Fig. 11 shows the PCM temperature contours at sections of top, middle and bottom of the PCM HX tank and at times of 30 s, 630 s, 3050 s, 5730 s and 6120 s during the discharging process. The inlet HTF temperature and flow rate are maintained at 10 °C and 0.1 L/s respectively. At the beginning of the discharging process (at 30 s), due to the high temperature difference between the PCM (40 °C) and inlet temperature (10 °C) and pure sensible heat transfer, the PCM liquid temperatures drop quickly in the areas close to the pipe outer surface especially for the first two pipes from the inlet. At 630 s, some areas around the pipes close to inlet have been solidified and the rest are approaching to be solidified. In addition, the PCM temperatures increase from right to left for each section following the same temperature profile of HTF flow. At mid of the discharging process (at 3050 s), the PCM temperature increases radially from each pipe outer surface

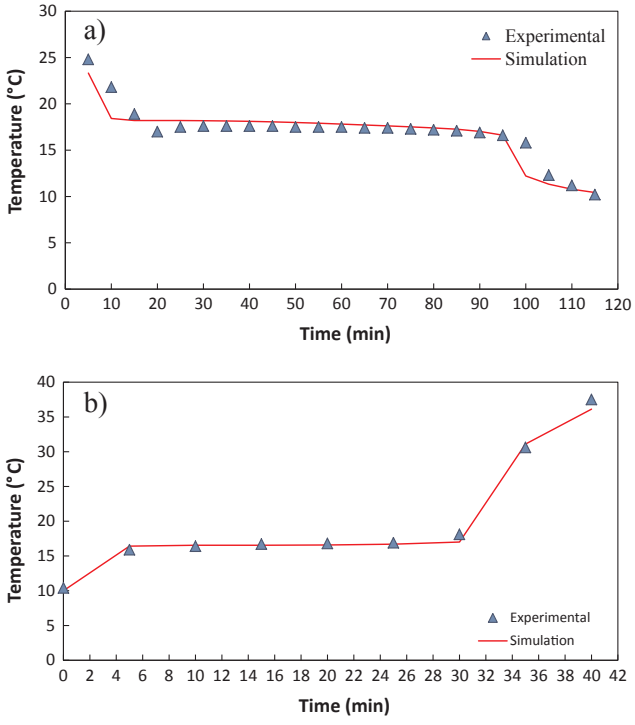

Fig. 8. PCM HX Model Validation – (a) discharging (b) charging.

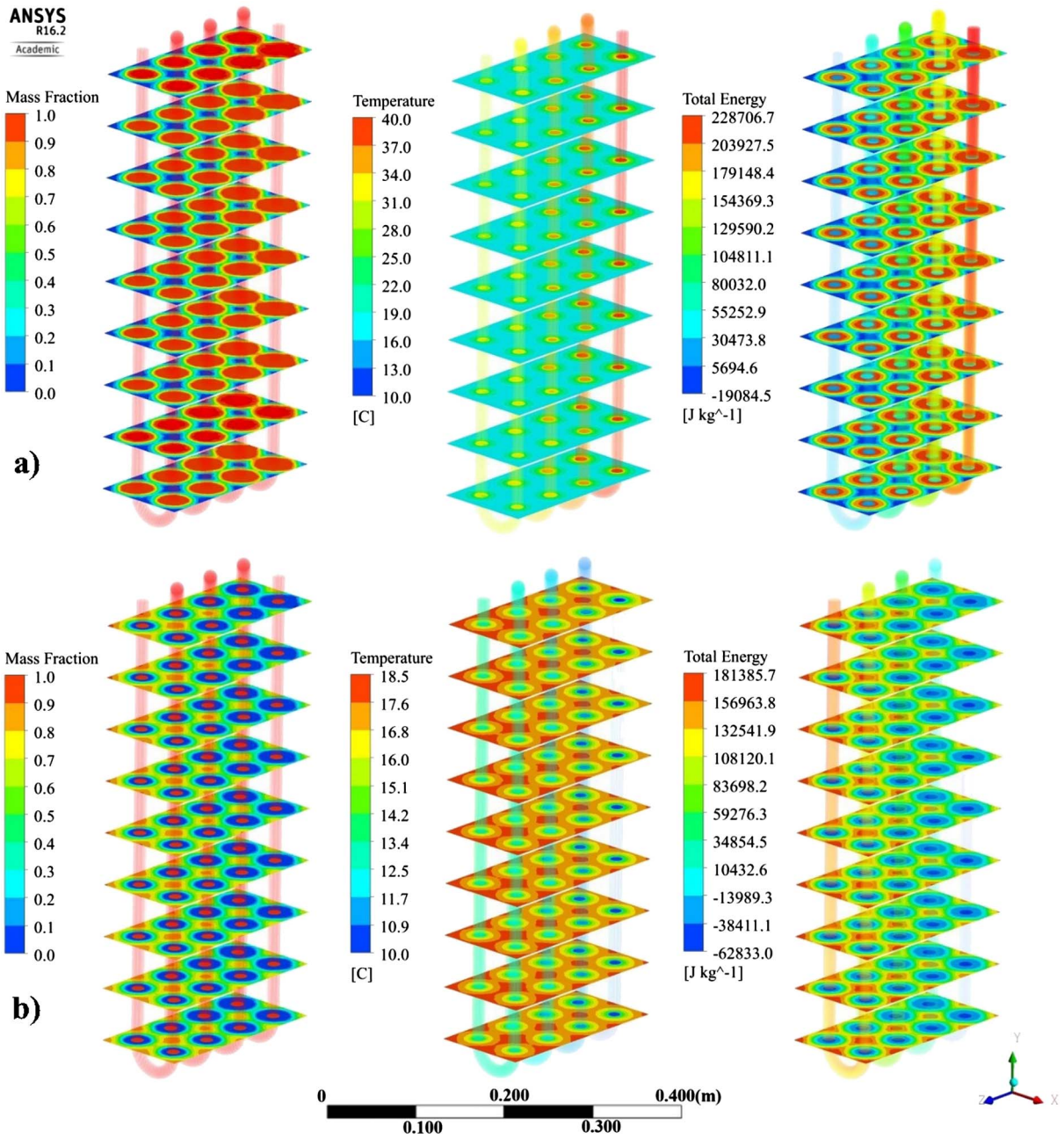

Fig. 9. Mass fraction, Temperature and total energy at the middle of operation – (a) charging process at 1050 s, (b) Discharging process at 3050 s.

and up to 50% around the pipes have been solidified. As explained earlier, this will add more thermal conduction resistance and thus lead to longer process time. By the end of solidification process (at 5730 s), it is noticed that over 75% of overall PCM in the tank is solidified and the rest of tank is still in transition states (between 15 and 17 °C). At time 6120 s when the discharging process ends, the PCM in the tank is completely solidified while the lowest and highest PCM temperatures are close to the inlet and outlet pipes respectively. Simultaneously, the HTF is heated up to approximately 12 °C at the PCM HX outlet.

4.2. Effect of HTF flow rate variation

With the developed and validated PCM HX CFD model, simulations are carried out at inlet temperatures of 10 ^{0}C and 40 ^{0}C during discharging and charging processes respectively. For each process, three HTF flow rates are applied: 0.1, 0.2 and 0.3 L/s based on the applicable operation of indirect solar assistant heat pump system where the PCM HX is fitted. It is expected that the higher HTF flow rate can enhance its convection flow heat transfer and thus speed up both the discharging and charging processes. For the PCM discharging process, the initial PCM temperature inside the tank is set to 40 ^{0}C. The temporal variations of PCM temperature and liquid fraction at the mid of tank can thus be simulated and shown in Fig. 12. From these simulation results, due to the larger temperature difference between HTF and PCM and small sensible heat transfer involved, the PCM can all quickly approach to transition temperature point. Although the higher HTF flow rate can speed up a bit this process, the temperature difference between PCM and HTF seems to dominate. In addition, since the main thermal resistance is on the PCM liquid side, the thermal resistance reduction on the HTF flow side due to the flow rate increase has little effect on the overall heat transfer during this period. After that, at each HTF flow rate, the PCM starts to transit phase from liquid to solid by releasing larger latent heat to the HTF and thus taking longer time to complete the phase change. Meanwhile, from heat transfer point of view, due to

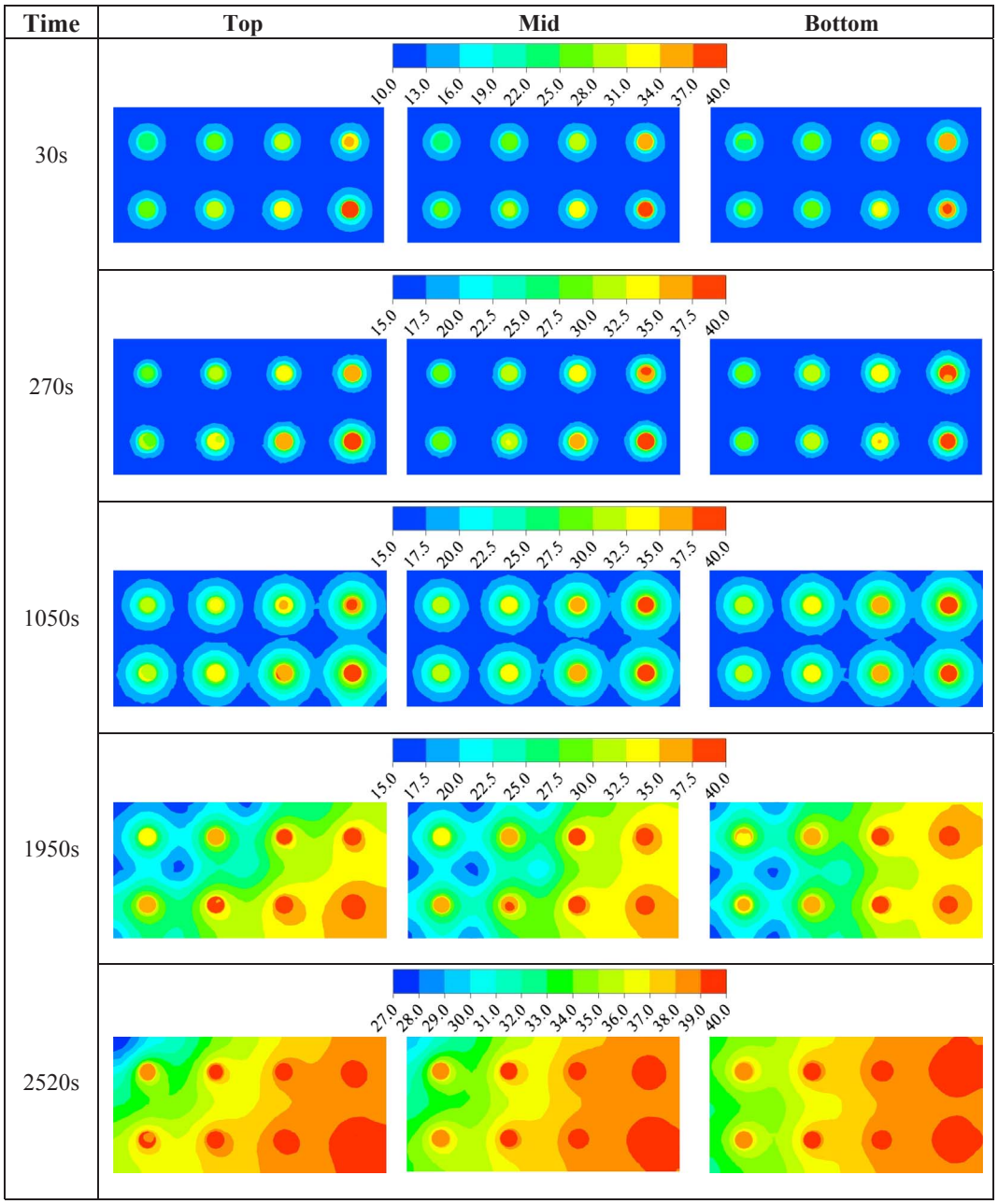

Fig. 10. Charging temperature (°C) timeline at flow rate 0.1 L/s.

the phase change involved, the heat transfer coefficient on the PCM is greatly improved such that the PCM side is not the main thermal resistance anymore. Therefore, the heat transfer enhancement on the HTF side due to the flow rate increase can significantly affect the overall heat transfer of the heat exchanger and thus greatly reduce the completion time of phase change. Once the PCM is solidified, the PCM temperature drops abruptly at the beginning due to the relatively low solid PCM thermal resistance and limited sensible heat transfer. However, with the reduction of the temperature difference between HTF and PCM, the heat transfer process is also reduced such that the PCM temperature decrease rate is also slowed down as shown in Fig. 12. Correspondingly, more time is needed for the PCM transition period and the time is greatly reduced when the HTF flow rate increases.

For the PCM charging process, the initial PCM temperature inside the tank is set to 10 ^{0}C. The temporal variations of PCM temperature and liquid fraction at the mid of tank can thus be simulated and shown in Fig. 13. Similar to the discharging process, at each HTF flow rate, the phase transition period from solid to liquid dominant the whole discharging period. Meanwhile, the higher HTF flow rate can enhance the overall heat transfer during the phase change period and therefore speed up the charging process.

4.3. Effect of HTF inlet temperature variation

As another important application, the developed CFD model is used to simulate the PCM discharging and charging processes at constant HTF flow rate (0.1 L/s) but varied inlet temperatures which are 5 ^{0}C, 10 ^{0}C and 15 ^{0}C for discharging process and 30 ^{0}C, 40 ^{0}C and 50 ^{0}C for charging process. The selections of these inlet temperatures are all applicable for the actual operation of indirect solar assistant heat pump system where the PCM HX is integrated. For the discharging process, the initial PCM temperature is set to 40 ^{0}C. The temporal variations of PCM temperature and liquid fraction at the mid of tank can thus be simulated and shown in Fig. 14. From these simulation results, due to

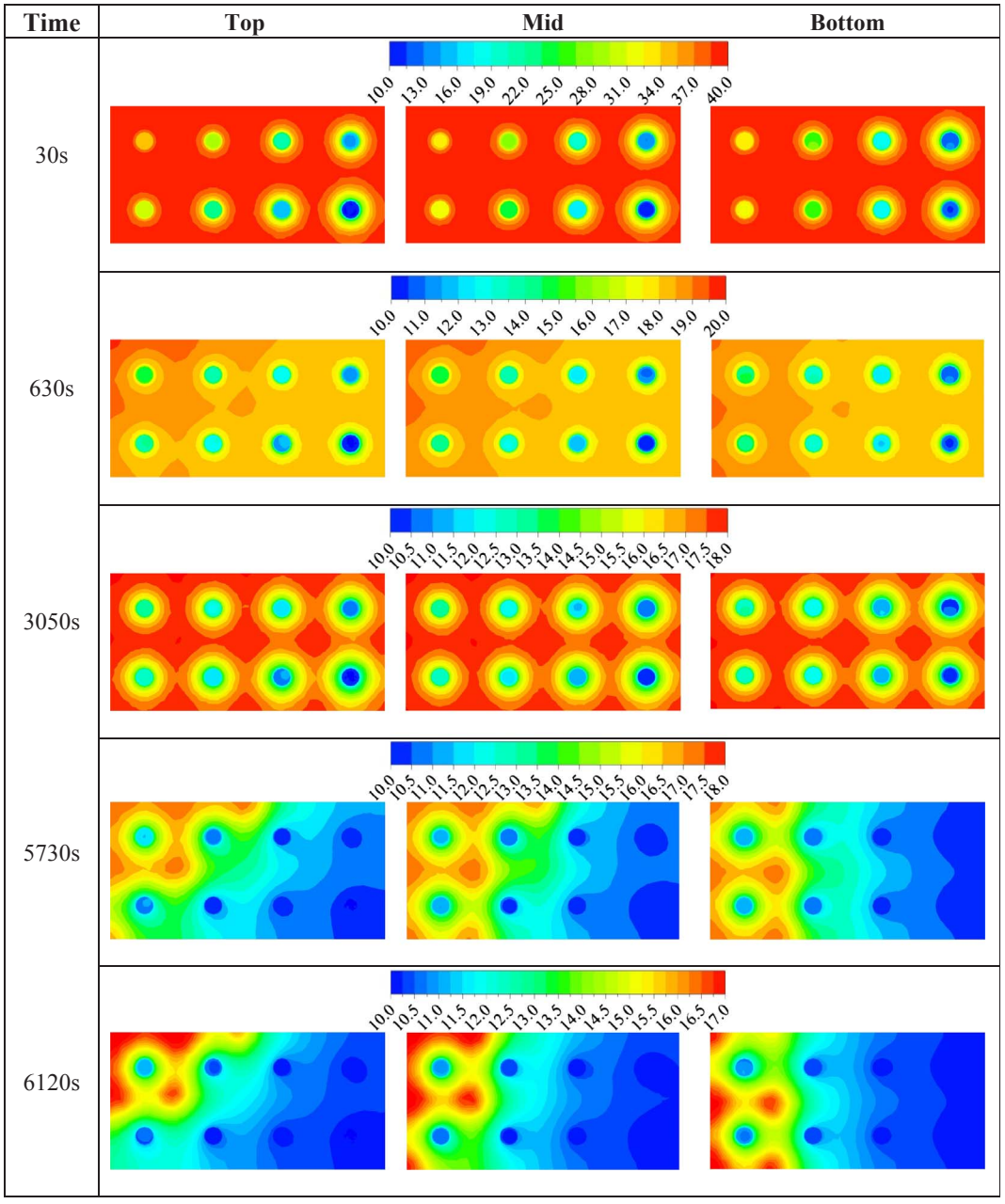

Fig. 11. Discharging temperature (°C) timeline at flow rate 0.1 L/s.

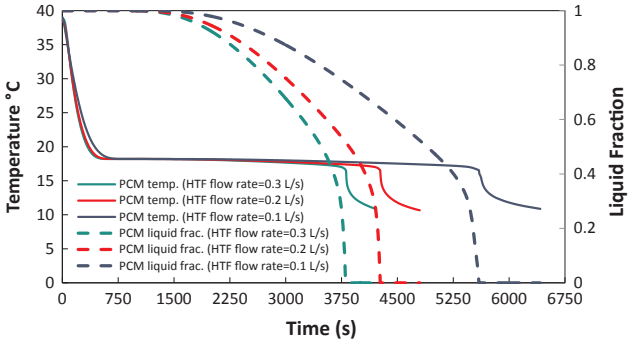

Fig. 12. Variations of PCM temperature and liquid fraction with time at the middle of PCM HX for different HTF flow rates during discharging processes.

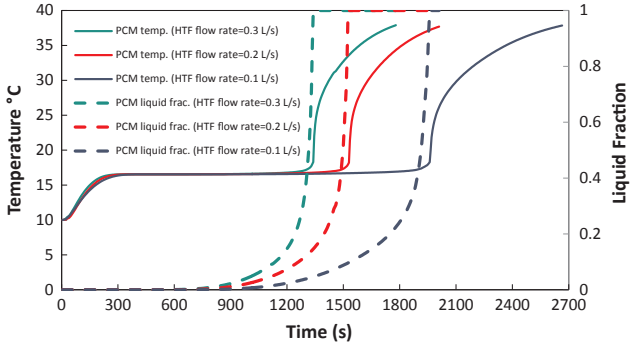

Fig. 13. Variations of PCM temperature and liquid fraction with time at the middle of PCM HX for different HTF flow rates during charging processes.

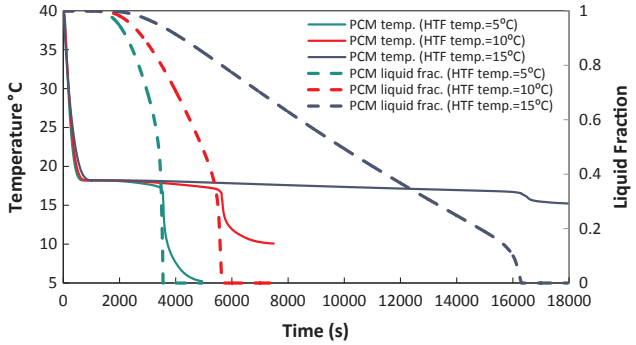

Fig. 14. Variations of PCM temperature and liquid fraction with time at the middle of PCM HX for different HTF temperatures during discharging processes.

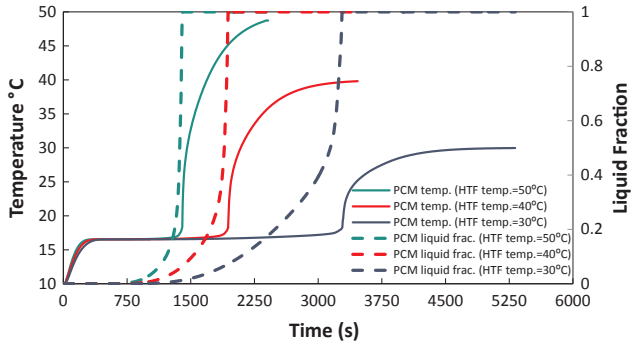

Fig. 15. Variations of PCM temperature and liquid fraction with time at the middle of PCM HX for different HTF temperatures during charging processes.

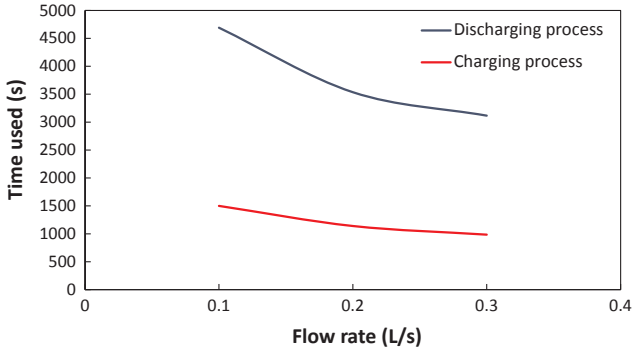

Fig. 16. Variations of solidification and liquidation times with different HTF flow rates during discharging and charging processes.

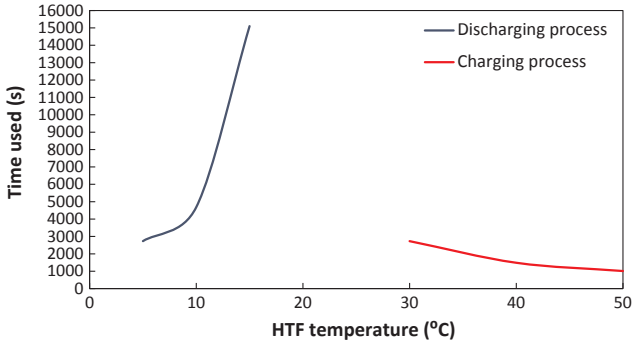

Fig. 17. Variations of solidification and liquidation times with different HTF temperatures during discharging and charging processes.

the significant temperature difference between HTF and PCM and small sensible heat transfer involved, the PCM can all quickly approach to transition temperature point. Although the lower HTF inlet temperature can speed up a bit this process, it is compromised by the relatively small sensible energy stored. After that, at each HTF inlet temperature, the PCM starts to transit phase from liquid to solid by releasing larger latent heat to the HTF and thus taking longer time to complete the phase change. However, the lower fluid inlet temperature can lead to higher temperature difference between PCM and HTF and therefore increase the heat transfer rate. At constant PCM latent heat energy, the phase transition period can be greatly reduced with higher heat transfer rate or lower HTF inlet temperature. Once the PCM is solidified, the heat transfer process is much quicker considering the small sensible energy stored.

For the PCM charging process, the initial PCM temperature inside the tank is set to 10 ^{0}C. The temporal variations of PCM temperature and liquid fraction at the mid of tank can thus be simulated at constant fluid flow rate but different inlet temperatures, as shown in Fig. 15. Similar to the discharging process, at each HTF inlet temperature, the phase transition period from solid to liquid dominant the whole charging period. Meanwhile, the higher HTF inlet temperature can enhance the overall heat transfer during the phase changer period and therefore speed up the charging process.

4.4. PCM solidification and liquidation times

As demonstrated in Sections 4.2 and 4.3, the PCM discharging and charging speeds at different operating conditions are determined mainly by the corresponding solidification and liquidation times required. To clarify these, based on the simulation results from Figs. 12 and 13, the variations of PCM discharging and charging times with various HTF flow rate but fixed HTF temperature (10 ^{0}C for discharging or 40 ^{0}C for charging) are calculated and shown in Fig. 16. It is revealed that both the PCM discharging and charging times decrease with higher HTF flow rate. However, at the same HTF flow rate, the required PCM discharging time is much larger than that of charging time with the reasons explained in Section 4.2. On the other hand, based on the simulation results from Figs. 14 and 15, the variations of PCM discharging and charging times with various HTF temperature but fixed HTF flow rate (0.1 L/s) are calculated and shown in Fig. 17. It is shown that the PCM discharging time needed increases with higher HTF temperature while the PCM charging time required decreases with the increased HTF temperature. Again, the required PCM discharging time is much larger than that of charging time with the reasons explained in Section 4.2.

5. Conclusions

Latent thermal energy storage technologies with PCMs are essential to be applied to solar thermal systems considering the intermittent nature of solar energy resource and requirement of system compactness. However, the PCM thermal conductivity needs to be greatly enhanced so as to speed up the processes of energy storage and release-ment. In this paper, a PCM HX is purposely designed, manufactured and installed in an indirect solar assistant heat pump system. The PCM HX consists of eight spiral-wired tubes and enclosed with metal sheets in which organic PCM is charged on the outer tube side with wire fins while heat transfer fluid (HTF) flowing through the tube side. The spiral-wired tube is firstly applied by this project into the heat transfer enhancement of the designed PCM HX. The special design of a spiral-wired tube can improve the thermal conductivity of PCM and allow free movement of PCM during phase change processes which could further enhance the heat transfer. Even so, further detailed evaluation and analysis are necessary. Correspondingly, to fully understand the dynamic charging and discharging processes of the PCM HX with spiral–wired tubes, a 3D CFD model of the heat exchanger has been

developed and validated with experimental results. It is found from the simulation results that at specific operating conditions the charging times are much faster than the discharging time. This is due to the contributions of convection heat transfer and buoyancy effect generated on the PCM side during charging or liquefying process. In addition, the HTF side temperature and flow rate can also affect the discharging and charging processes of the PCM HX. The higher HTF inlet flow rate can speed up both discharging and charging processes. Meanwhile, the lower and higher HTF inlet temperatures can improve the discharging and charging processes respectively. However, the effects of these parameter changes in the sensible heat storage and releasement are not significant. The simulation results can help to understand the dynamic charging and discharging processes of the PCM HX and instruct efficiently the operation of the heat exchanger and its integration with the solar system.

Acknowledgements

The authors would like to thank the Engineering and Physical Science Research Council, Spirotech b.v. the Netherlands, and Kingspan UK for supporting this research work.

References

[1] Ibrahim NI, Al-Sulaiman FA, Rahman S, Yilbas BS, Sahin AZ. Heat transfer enhancement of phase change materials for thermal energy storage applications: a critical review. Renew Sustain Energy Rev 2017;2017(74):26–50.
[2] Edem N'tsoukpoe K, Liu H, Le Pierrè N, Luo L. A review on long-term sorption solar energy storage. Renew Sustain Energy Rev 2009;13:2385–96.
[3] Abhat A. Low temperature latent heat thermal energy storage: heat storage materials. Sol Energy 1983;30:313–32.
[4] Zalba B, Marin JM, Cabeza LF, Mehling H. Review on thermal energy storage with phase change: materials, heat transfer analysis and applications. Appl Therm Eng 2003;23:251–83.
[5] Bruno F. Using phase change materials (PCMs) for space heating and cooling in buildings. In: The 2004 AIRAH Performance Enhanced Buildings Environmentally Sustainable Design Conference; 2004. p. 26–31.
[6] Alva G, Liu L, Huang X, Fang G. Thermal energy storage materials and systems for solar energy applications. Renew Sustain Energy Rev 2017;68:693–706.
[7] Jegadheeswaran S, Pohekar SD. Performance enhancement in latent heat thermal storage system: a review. Renew Sustain Energy Rev 2009;13:2225–44.
[8] Kenisarin M, Mahkamov K. Solar energy storage using phase change materials. Renew Sustain Energy Rev 2007;11:1913–65.
[9] Rathod MK, Banerjee J. Numerical investigation on latent heat storage unit of different configurations. Int J Mech Aerospace, Ind Mechatron Manuf Eng 2011;5. 652–557.
[10] Tian Y, Zhao CY. A numerical investigation of heat transfer in phase change materials (PCMs) embedded in porous metals. Energy 2011;36:5539–46.
[11] Agyenim F, Eames P, Smyth M. A comparison of heat transfer enhancement in a medium temperature thermal energy storage heat exchanger using fins. Sol Energy 2009;83:1509–20.
[12] Al-Abidi AA, Mat S, Sopian K, Sulaiman MYY, Mohammad AT. Internal and external fin heat transfer enhancement technique for latent heat thermal energy storage in triplex tube heat exchangers. Appl Therm Eng 2013;53:147–56.
[13] Liu Z, Sun X, Ma C. Experimental investigations on the characteristics of melting processes of stearic acid in an annulus and its thermal conductivity enhancement by fins. Energy Convers Manag 2005;46:959–69.
[14] Medrano M, Yilmaz MOO, Nogués M, Martorell I, Roca J, Cabeza LF. Experimental evaluation of commercial heat exchangers for use as PCM thermal storage systems. Appl Energy 2009;86:2047–55.
[15] Esen M, Ayhan T. Development of a model compatible with solar assisted cylindrical energy storage tank and variation of stored energy with time for different phase-change materials. Energy Convers Manage 1996;37:1775–85.
[16] Esen M, Durmus A, Durmus A. Geometric design of solar-aided latent heat store depending on various parameters and phase change materials. Sol Energy 1998;62:19–28.
[17] Esen M. Thermal performance of a solar-aided latent heat store used for space heating by heat pump. Sol Energy 2000;69:15–25.
[18] Fluent INC 2016; Fluent User Guide 17.0.
[19] Assis E, Katsman L, Ziskind G, Letan R. Numerical and experimental study of melting in a spherical shell. Int J Heat Mass Transfer 2006;50. 1790-180.
[20] Zhou T, Liu X, Li Y, Sun Z, Zhou J. Dynamic measurement of the thermal conductivity of phase change materials in the liquid phase near the melting point. Int J Heat Mass Transfer 2017;111:631–41.
[21] Youssef W, Ge YT, Tassou SA. Effects of latent heat storage and controls on stability and performance of a solar assisted heat pump system for domestic hot water production. Sol Energy 2017;150:394–407.
[22] Incropera FP, DeWitt, DP, Bergman TL, Lavine AS. Fundamentals of heat and mass transfer. 6th ed. John Wiley; 2007.
[23] Ye W-B, Zhu D-S, Wang N. Numerical simulation on phase-change thermal storage/release in a plate-fin unit. Appl Therm Eng 2011;31:3871–84.
[24] Zhang Z, Zhang W, Zhai Z, Chen QY. Evaluation of various turbulence models in predicting airflow and turbulence in enclosed environments by CFD: part 2—comparison with experimental data from literature. HVAC&R Res 2007;13:871–86.